Astronomy & Astrophysics manuscript no. ArticlenCours
June 20, 2011
© ESO 2011

Enhancement of images obtained with cophased stellar interferometers and hypertelescopes

Inpainting the Fourier space using the Richardson-Lucy algorithm

C. Aime[1], H. Lantéri[1], M. Diet[1], and A. Carlotti[1,2]

1 : Université de Nice Sophia-Antipolis, Centre National de la Recherche Scientifique, Laboratoire Fizeau, Observatoire de la Côte d'Azur, Parc Valrose, 06108 Nice
2 : Princeton University, Mechanical & Aerospace Engineering, Olden street, Princeton, 08544 NJ, USA
e-mail: claude.aime@unice.fr, henri.lanteri@unice.fr, megan_83@hotmail.fr,acarlott@princeton.edu

June 20, 2011

ABSTRACT

Aims. This paper describes the application of the classical Richardson-Lucy iterative deconvolution technique to improve images obtained with cophased diluted apertures and hypertelescopes. It makes it possible to perform a comparison between the two modes of operation of array of telescopes.
Methods. The principles of image formations with an array of telescopes operated in the Fizeau mode and in Michelson mode (hypertelescope) are briefly presented. The procedure is described as an inversion of the Fourier plane angular spectra. The principle of densification in the Fourier plane is illustrated on the example of a simple redundant square array of 3×3 telescopes. A non-redundant array of 25 telescopes is used for comparison of the images obtained by the two techniques, before and after deconvolution. Simulations are made for noiseless images and for low light level images, in a photodetection regime.
Results. The Richardson-Lucy algorithm allows bringing together the replicas of the Fizeau image to a single high quality image. It fails to give good results with the densified image. However, the images obtained with an hypertelescope may be rediluted in a post processing in order to retrieve the same high quality images than in the direct procedure while retaining the benefit of hypertelescopes to image acquisition with detectors with a small number of pixels.

Key words. Instrumentation: high angular resolution – Instrumentation: interferometry – Techniques: high angular resolution – Techniques: interferometry

1. Introduction, reformater + refs

Since Michelson (1920) pioneering observations, optical interferometers have been used to obtain high angular information on stellar structures. It took a long time to go from the early measurement of the diameter of Betelgeuse by Michelson & Pease (1921), to the use of two coherent telescopes (Labeyrie (1975), Mourard et al. (1994)) up to the development of recent stellar interferometers such as CHARA (ten Brummelaar et al. (2005), Mourard et al. (2009)) and VLTI (Ohnaka et al. (2011)).

The results of optical interferometers are however not yet to compare with imaging capabilities obtained in radio astronomy, (reference VLA, Lofar, FasR...), but times are not as distant as one might consider similar situations. For ground based observations, the problems are still linked with an imperfect correction of the effect of atmospheric turbulence, although the progress in adaptive optics, combined with the use of phase closure techniques, can solve most of the problems. The array configuration, number and size of telescopes is a key issue in interferometric imaging (references bouquin Ukraine et autres).

The question will arise with interferometers whether the observers seek to obtain snapshot images or if it will be possible to use super synthesis techniques, in which the information on the object will be sequentially obtained with different aperture configurations. Super-synthesis is a powerful tool at the basis of radioastronomical results that assumes that the apertures reconfiguration will be made in a time short enough compared to the astronomical object evolution.

Whatever the procedure, the result obtained directly from arrays of diluted apertures will only provide the observers with a dirty-map, as called by radioastronomers where algorithms such as CLEAN (reference) are used to recover a scientifically exploitable image. As we will see in section 4, we will prefer to use the Richardson-Lucy algorithm instead of CLEAN.

The main object of this paper is to perform a comparison of focal plane images obtained after deconvolution for two modes of operation of cophased diluted apertures. The first mode of operation, called the Fizeau mode, is the usual mode in which the geometry of the apertures seen from the stellar source is conserved down to the common focus of the array. The second mode of operation, called the Michelson mode, is the mode in which the apertures are densified. The system is called hypertelescope. Densification is equivalently obtained either by making closer the individual apertures by means of periscopical mounts, or by enlarging the sizes of the individual apertures by means of inverted Galilean telescopes. The technique utilized to deconvolve the images is the classical Richardson-Lucy technique. Tests are performed on noiseless images and on images obtained at low light level, in a photodetection regime.

Send offprint requests to: C. Aime

A CASER AUTREMENT:

This illustration is the case to remind that a stellar interferometer generally only transmit non-contiguous areas of the spectrum, with as much missing areas than the elementary apertures are small and distant to each other. The apparent angular size of the astronomical object will result in more or less fine structures in the Fourier plane, the larger the object, the finer the observed structure. Whether the areas transmitted by the diluted array allows a good sampling of the image spectrum is a question that we shortly consider further on in the paper.

The hypertelescope we consider is the one that produces a densification of the OTF, and not of the aperture. This is to prevent overlapping of parts of the spectrum originating from different frequencies, as discussed by Aime (2008). This manage the possibility of redilution in a post processing of the image and the recovering of the object-image convolution relationship, as already described by Tallon & Tallon-Bosc (1992).

The paper is organized as follows. Theoretical aspects leading to the formation of an image with an interferometer and an hypertelescope, at high light level and at photon counting level are given in section 2. A simple illustration of the densification procedure is given for the case of a redundant array of 3×3 telescopes in section 3, and then detailed illustrations of images are given for the case of a non-redundant array of 25 telescopes. After a brief presentation of the Richardson-Lucy technique, section 4 presents the image enhancement that can be obtained with this technique. Section 5 presents a discussion and gives a conclusion.

2. Theoretical aspects of image formation and detection

2.1. Image formation with a cophased stellar interferometer

In this section we give the notations and mathematical formalism for the formation of an image with a cophased stellar interferometer operated in Fizeau mode, i. e. with no modification of the aperture configuration. For simplicity, we restrict our analysis to the case of perfectly cophased telescopes operated outside the earth atmosphere. To further simplify the presentation, all elementary apertures will be taken identical and we will also assume observations made in monochromatic light. In what follows, the aperture is denoted by $P(r)$, with $r(x,y)$, and there is no difference in the first four equations whether $P(r)$ refers to a single aperture or to an array of apertures interfering coherently at a common focus. The specificity of diluted apertures is introduced later.

The observed image $I(\alpha)$ in the focal plane of a telescope is given by the convolution relation

$$I(\alpha) = R(\alpha) * O(\alpha), \tag{1}$$

where $O(\alpha)$ is the perfect geometrical image of the object in the focal plane, the symbol $*$ denotes the two-dimensional convolution applied on components of the angular coordinates $\alpha(\alpha_x, \alpha_y)$ on the sky, and $R(\alpha)$ is the point spread function (PSF)

$$R(\alpha) = \frac{1}{S\lambda^2}|\hat{P}(\frac{\alpha}{\lambda})|^2, \tag{2}$$

where λ is the light wavelength, and S is the area of the aperture transmission, and $\hat{P}$ stands for the two-dimensional Fourier transform of P. With this definition, the PSF is normalized so that its two-dimensional integral performed over α is equal to unity. In the Fourier plane, the object image relationship appears as a linear filtering

$$\hat{I}(u) = T(u)\ \hat{O}(u), \tag{3}$$

where $u(u_x, u_y)$ denotes angular frequencies, $\hat{O}(u)$ is the image transform, and $T(u)$ is the optical transfer function (OTF), a complex function that describes the transmission in amplitude and phase of the angular frequencies. Taking the Fourier transform of Eq. 2, the OTF can be written as the aperture autocorrelation function

$$T(u) = \frac{1}{S}\int P(r)P^*(r-\lambda u)d^2r, \tag{4}$$

where $P^*(r)$ is the complex conjugate of $P(r)$. For a the perfect telescopes we consider in this study, $P(r)$ is real and $T(u)$ is an even, real and positive function. It is normalized so that $T(0) = 1$. For a monolithic aperture, $T(u)$ corresponds to a two-dimensional low pass filter that transmits continuously all frequencies from zero up to the cutoff limiting border.

As already indicated, the above relations are valid regardless of the fact that $P(r)$ is a monolithic aperture or a collection of diluted apertures. For K (non-overlapping) identical elementary apertures of transmissions $P_0(r)$, centered at positions $r_k = (x_k, y_k)$, the transmission $P(r)$ can be written as

$$P(r) = P_0(r) * \sum_{k=1}^{K}\delta(r-r_k), \tag{5}$$

Making use of Eq. 2 the PSF becomes

$$R(\alpha) = \frac{1}{S\lambda^2}|\hat{P_0}(\frac{\alpha}{\lambda})|^2|\sum_{k=1}^{K}\exp(-\frac{2i\pi}{\lambda}(\alpha.r_k))|^2, \tag{6}$$

where $\alpha.r_k = \alpha_x x_k + \alpha_y y_k$, and $S = KS_0$, S_0 being the area of an elementary aperture. This relation takes the form of the well known product of diffraction and interference terms. The OTF $T(u)$, Fourier transform of $R(\alpha)$, can be written as the convolution product of two terms

$$T(u) = T_0(u) * G(u) = T_0(u) * (\delta(u) + \frac{1}{K}\sum_{l=1}^{K}\sum_{k\neq l}^{K}\delta(u-u_{kl})), \tag{7}$$

where $T_0(u)$ is the OTF of an elementary aperture, all apertures being assumed identical, and $G(u)$ is the autocorrelation function of the positions of the apertures. This latter function gives the positions of the centers of the transmitted frequency domains, and can be computed as the differences of positions between elementary apertures $u_{kl} = (r_k - r_l)/\lambda$ in units of the light wavelength.

To simulate the image $I(\alpha)$ observed in the focal plane of a telescope or an array of telescopes, rather than perform the convolution of Eq. 1, it is more convenient to calculate first the quantity $T(u)\hat{O}(u)$ and then to recover the focal plane image by an inverse Fourier transform

$$I(\alpha) = \mathcal{F}^{-1}\left[T(u)\hat{O}(u)\right] \tag{8}$$

For an usual monolithic aperture, the PSF is a compact spot and the resulting image $I(\alpha)$ is the conventional blurred, low resolution version of $O(\alpha)$. The image can be used as it is for a scientific analysis, although a deconvolution can improve the observation. For an array of telescopes, the problem is different. The PSF is somewhat chaotic, the intensity is no more concentrated in a single spot. Ghosts are present in the images that may appear as an ensemble of replicas, depending on the configuration of the array. The technique we examine in the next section is a way to recover by means of an hardware optical operation a usable astronomical image from an array of telescopes.

2.2. Image formation with a cophased hypertelescope

As already indicated, the principle of hypertescope was proposed by Labeyrie (1996)) to recover directly snapshot images from a diluted array of telescopes. For example, if the array takes the form of a two dimensional highly diluted grid, the raw focal plane image shows a large number of replicas of the object, and the use of an hypertelescope makes it possible to bring together all replicas in a single image. So doing, it has the advantage of requiring detectors with a reduced number of pixels, which can be very interesting considering in the Fizeau mode the apparent useless dispersion of the photons over the multiple replicas of the astrophysical image of interest. The interest to regroup all photons in a single image is undeniable, and can even change the nature of the required detectors.

The technique consists of the use of optical instrumentation so that from the final focal plane the aperture resemble as much as possible to a monolithic aperture. The operation called densification is obtained by putting side by side the images of subapertures using the periscopic principle of Michelson. In this operation, the pattern of sub-pupil centers must remain identical in the entrance and exit pupils, to an homothetic transformations. An equivalent result can be obtained by applying a magnification of the elementary apertures by means of inverted Galilean telescopes. The aperture transmission $P(r)$, after the densification is applied, is seen as the densified transmission $P'(r)$ of the form:

$$P'(r) = P_0(r) * \sum_{k=1}^{K} \delta(r - r'_k), \tag{9}$$

where $r'_k = (x'_k, y'_k)$ are the new positions of the centers of the apertures, the set of positions r'_k forming an homothetic smaller image of the r_k that appear in Eq.5.

The formulation of the process of image formation with an hypertelescope in the Michelson mode is more tricky than in the Fizeau mode. As a result of the transformation, the point spread function depends on the position of the point source on the sky, as described by Labeyrie (2007), Lardière et al. (2007), Patru et al. (2008) and Patru et al. (2009). From a numerical point of view, this makes it difficult to simulate the final image because the relation of convolution between the object and the image must be replaced by a Fredholm equation in which the PSF varies with the position of the point source in the field.

The numerical implementation of that two dimensional Fredholm equation is heavy (references). Hopefully, there exists a very effective way to simulate hypertelescope images. The procedure was described by Aime (2008) making use of the approach of Tallon & Tallon-Bosc (1992). These authors developed a complete theory of what that was not yet called densification in their study of the object-image relationship in Michelson stellar interferometry, four years before the proposal of hypertelescopes. In what follows we will make plenty use of their work. The main result of Tallon & Tallon-Bosc (1992) is to show that in the Michelson configuration the part of the Fourier plane transmitted by a pair of telescopes around the frequency $u_{kl} = (r_k - r_l)/\lambda$ is shifted as a whole to a lower frequency $u'_{kl} = (r'_k - r'_l)/\lambda$, without any modification of the frequency transmission in modulus and phase. Because with a hypertelescope the transformation of the centers of transmission domains is homothetic, for all k and l, we have $u'_{kl} = u_{kl}/\gamma$, where γ is the densification parameter. Rewriting Eq.12 of Tallon & Tallon-Bosc (1992) to have the OTF equal to 1 at the origin, we have

$$\hat{I'}(u) = T_0(u)\hat{O}(u) + \frac{1}{K}\sum_{l=1}^{K}\sum_{k\neq l}^{K} T_0(u - u'_{kl})\hat{O}(u - u'_{kl} + u_{kl}), \tag{10}$$

and the hypertelescope image $I'(\alpha)$ is obtained as the inverse Fourier transform

$$I'(\alpha) = \mathcal{F}^{-1}[\hat{I'}(u)] \tag{11}$$

Provided that the densification can be done in a legitimate manner for a given astronomical object and array configuration, the effect of densification of the image can be seen as a zoom applied to the image replicas so that to isolate a central image collecting all the light. As shown by Aime (2008), the densification should refer to the OTF rather than the aperture. An illustration of direct and densified images are shown in the next section.

2.3. Principle of the simulation of photodetected images

The procedure we use to simulate the photodetected images derives from the semi-classical theory of photodetection. This theory (REF GOODMAN Statistical optics) assumes a classical propagation of the light down to the detector, using the Huygens-Fresnel theory of wave propagation, the quantum part being introduced in the transformation of the energy which arrive in a pixel into photoelectrons. Assuming that an integrated energy m arrives in a pixel, m being a real positive number measured in units of photon energy $h\nu$, the possible integer number of photoelectrons n can be simulated using a random draw that obeys the Poisson distribution of mean m, i.e. a law of the form $P(n/m) = e^{-m}m^n/n!$.

From a practical point of view, we start from a discrete representations of the deterministic images $I(\alpha)$ and $I'(\alpha)$. We associate the pixels of these images with the elements of a 2D detector. In what follows we work with simulated images of 1024×1024 pixels. We assume that a total number N of photons arrive in average in an image. Knowing that we can derive the mean number of photons m_{ij} in a pixel of the image, with $i = 1, 1024 \times j = 1, 1024$ in our simulations. For that, the noiseless images $I(\alpha)$, or $I'(\alpha)$, are simply normalized so that the sum of all m_{ij} in each image equals N. Using this procedure, an almost infinite number of photodetected images, that we denote as $I_p(\alpha)$ and $I'_p(\alpha)$ in our paper, can be simulated from the deterministic images. The reader should note that the total total number of photons in the images is not exactly N, but fluctuates around N with a standard deviation of $\sqrt{N}$.

3. Numerical simulation of the images

A block-diagram of the simulations performed to obtain the images observed at the focus of a cophased stellar interferometer and an hypertelescope is given in **Fig.1**. The inputs are the astronomical object $O(\alpha)$ and the aperture array $P(r)$, leading to the MTF $T(u)$ through the autocorrelation function of the aperture, in units of the wavelength. The product $T(u)\hat{O}(u)$ gives the image transform $\hat{I}(u)$. The inverse Fourier transform of this quantity gives the image $I(\alpha)$ observed at the stellar interferometer focus. The hypertelescope image $I'(\alpha)$ is obtained through the image transform densification described in Eq.10. The procedure of densification, which is a complex non-linear process, will be explained on a simple pedagogical example. The photodetected images $I_p(\alpha)$ and $I'_p(\alpha)$ are obtained implementing the Poisson procedure described above. As already indicated, all outputs of this diagram corresponds to images that are obtained through the optics of the instruments.

To obtain the hypertelescope image, it is necessary to have a very good sampling of the Fourier plane to facilitate the frequency translations described in Eq.10, from $\hat{I}(u)$ to $\hat{I'}(u)$ in the diagram of Fig.1. For that, we use zero padding of the discrete

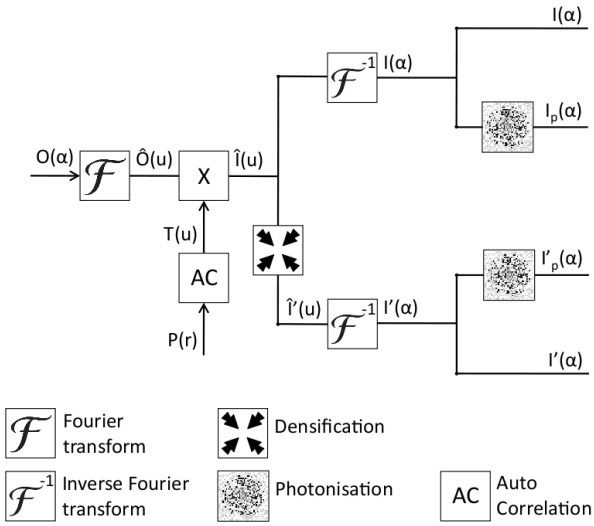


Fig. 1. Block-diagram of the numerical simulation giving the interferometric and hypertelescope images at high light level ($I(\alpha)$ and $(I'(\alpha))$ and in photodetection mode ($I_p(\alpha)$ and $(I'_p(\alpha))$.

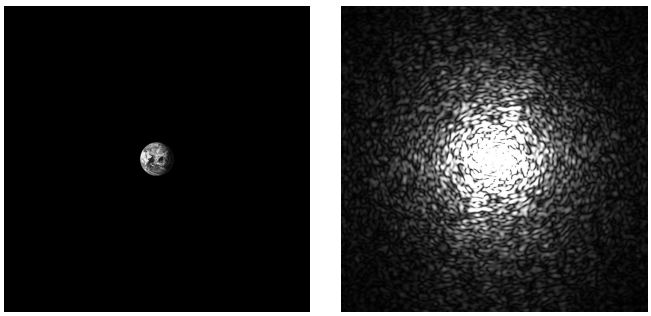


Fig. 2. Left: an Earth image of about 128×128 pixels is zero padded in an array of 1024×1024 pixels. Right: modulus of its Fourier transform (the zero frequency is at the center of the figure)

.

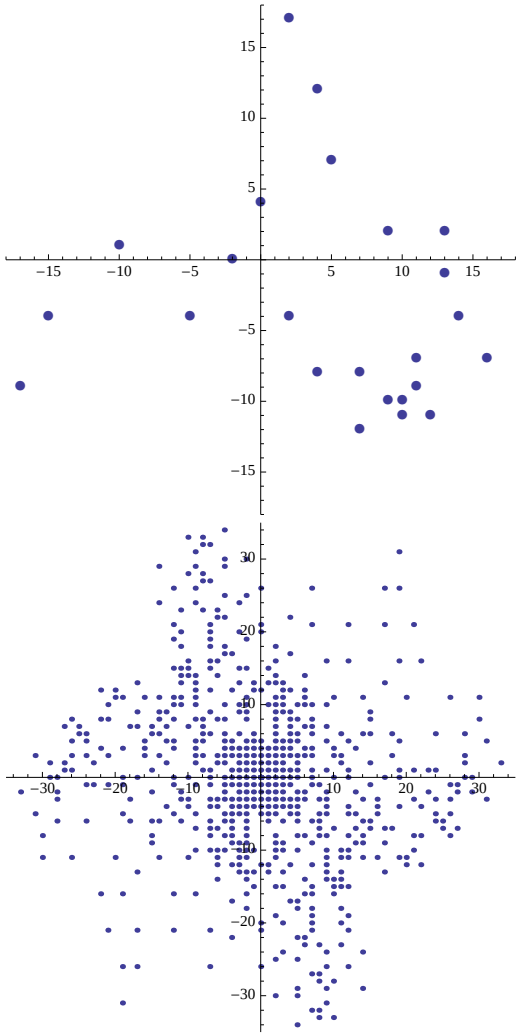


Fig. 3. An example of a possible configuration of 25 point-like non-redundant apertures (top) set on a square grid and represented here for $d = 1$, and its corresponding autocorrelation function $G(u)$ (bottom) made of 601 positions, in angular frequency units of d/λ.

image $O(\alpha)$. **Fig.2** shows the example of an Earth image of about 128×128 pixels embedded in an array of 1024×1024 zeroes. The modulus of its (discrete) Fourier transform $\hat{O}(u)$ is also shown in the figure.

The choice of a configuration of telescopes for $P(r)$ is a complex subject that is beyond the scope of this paper. The illustration of the effect of the Richardson-Lucy algorithm (RLA) on direct interferometric Fizeau images and on hypertelescope images can be made on any configuration, provided that this configuration is such that a densification can be possible. For example it is not possible to densify a configuration in which two telescopes are already contiguous.

In this paper we have considered a non-redundant array of $K = 25$ identical circular apertures of diameter D of minimal distances between them that is a multiple of d, in x and y. This configuration makes it possible to obtain images good enough for a simple visual interpretation of the reconstruction algorithm. We consider two values for d in the simulations. Of course other configurations could be easily investigated.

In **Fig.3** we show an example of positions r_k corresponding to a non redundant array of 25 apertures (top figure). The figure is drown in units of d, or equivalently for $d = 1$. The function $G(u)$ defined in Eq.7 as the autocorrelation of the positions of the

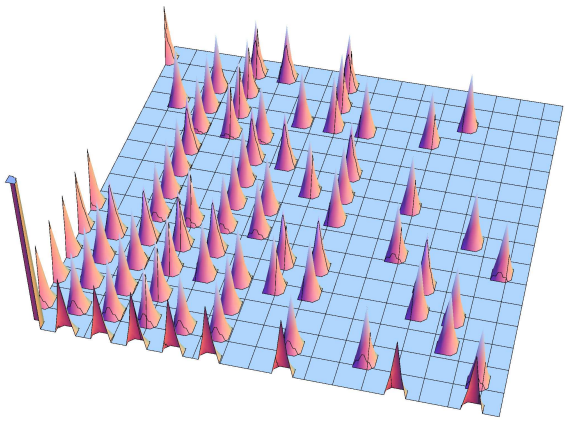


Fig. 4. 3D representation of a small central region of $T(u)$ for the array shown in Fig.2, with $d = 7$ frequels. The elementary MTF $T_0(u)$ spreads over 3 pixels. The region shown here corresponds to low frequencies values for u_x and $u_y \geqslant 0$.

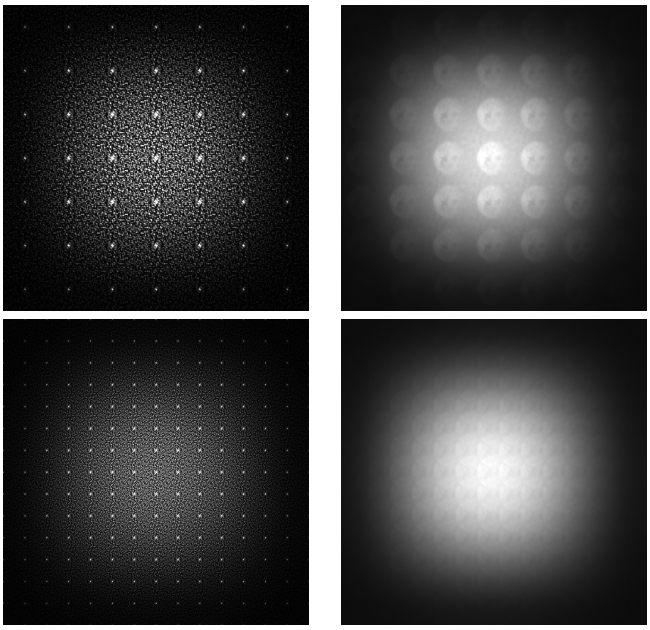


Fig. 5. PSFs $R(\alpha)$ (left) and focal plane images $I(\alpha)$ (right) for the 25 apertures non-redundant array for the object of Fig. 1. Images are for d =7 (top) and 14 (bottom). Replications of the object overlap in this latter case.

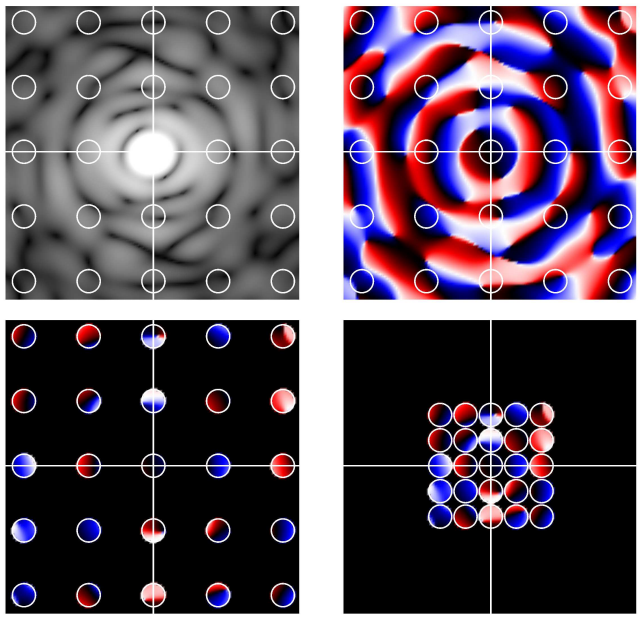


Fig. 6. Top: Central zone (128×128) of the object spectrum of Fig.2 in modulus (left) and argument (right), with superimposed circular regions of the 3×3 MTF array. Zero frequency is at lines intersection. Bottom: the densification operation (illustrated on arguments), from (left) the array MTF spectrum $\hat{I}(u)$ to (right) the hypertelescope $\hat{I}'(u)$. Color scale for argument is black (0), white ($\pm\pi$), blue ($-\pi/2$), and red ($\pi/2$).

elementary apertures is also given in this figure. In the frequency plane, this function is easily computed as the position differences between the r_k, expressed in units of the wavelength. Since the array is fully non-redundant, there are 601 regions of the Fourier plane transmitted by the array. One is the region around the zero frequency for which all apertures contribute, and $K(K-1) = 25 \times 24 = 600$ regions corresponding of couples of apertures, all transmitted with the amplitude $1/K = 1/25$, half of them corresponding to symmetric positions. Within the framework of our simulation, it is more convenient to use integer values for d. We have made two sets of simulation, for $d = 7$ and 14 units.

To obtain $T(u)$ we perform the convolution of $G(u)$ with $T_0(u)$. We use a telescope diameter D so that $T_0(u)$ spreads over 3 frequels squared. A close-up of the resulting OTF $T(u)$ for $d = 7$ is shown in **Fig.4**. The region represented there show the low frequency part (where the transmission is dense) covering about 80 out of the 600 frequencies regions transmitted by the 25 apertures telescope, in the central part of the Fourier plane, for positive values of u_x and u_y, including the zero frequency. With our normalization used $T(0) = 1$ and all other elementary peaks rise to $1/25$.

3.1. Images in Fizeau mode

Fig.5 shows the PSF and the corresponding observed focal plane images of the object of Fig.2 for the array represented in Fig.3 for $d = 7$ and 14. Since the array fill rather regularly a low frequency square grid, the corresponding focal plane images show an ensemble of pics. Because there are gaps in the grid coverage in the MTF, a diffuse speckle-like pattern is also present in the PSF. The focal images, result of the convolution of the object and the PSF, appear as en ensemble of object replicas superimposed to a cloudy background. For $d = 7$, the images of the Earth-like planet are clearly separated, while for $d = 14$ they overlap.

Following Aime (2008), a way to interpret the images is to make reference to the Shannon theorem, by reversing the usual

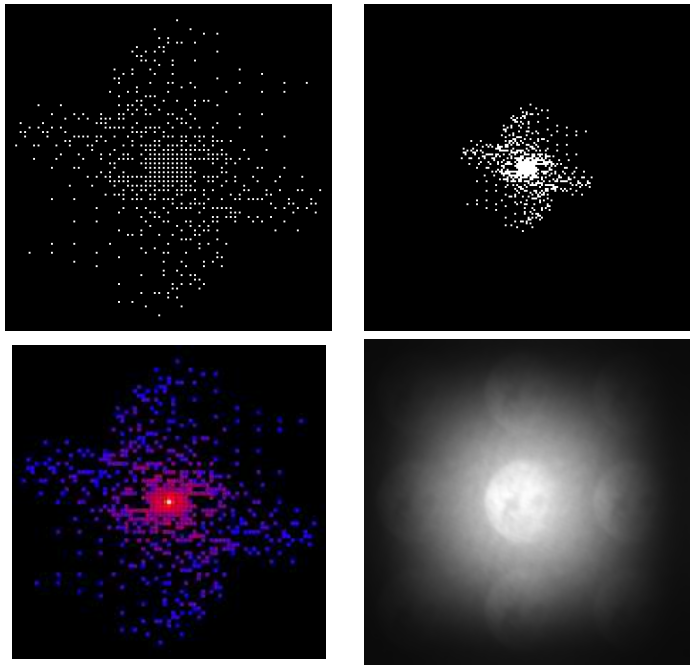


Fig. 7. Stages for the obtention of the hypertelescope image. Top: illustration of the densification of the Fourier space. Bottom: modulus of the densified image Fourier spectrum and the final focal plane image.

two spaces. With $d = 7$, the Fourier space is correctly sampled, while it appears under sampled for $d = 14$. From that we can anticipate a better recovery of the original object from the lower resolution array when a deconvolution procedure will be applied.

3.2. Images in Hypertelescope mode

The imaging process in an hypertelescote is a delicate process that deserves a particular attention, as already indicated. For that, before to apply the densification to the 25 apertures array, we illustrate the simulation on the simple example of a fully redundant square array of 9 telescopes, in a 3×3 configuration. As shown in the block-diagram of Fig.1, we start first from $\hat{I}(u)$ of the Fizeau array. Applying the autocorrelation function to the 3×3 array, it is easy to show that it will transmit 25 regions of the Fourier plane. These regions are represented in **Fig.6** as white circles superimposed to the modulus and argument of $\hat{O}(u)$. For clarity of the representation, we assume that only the central region of 128×128 frequency elements (frequels) of the Fourier plane shown in Fig. 1 is concerned by the array transmission.

The bottom images of Fig.6 illustrate the densification operation of the MTF. The representation is shown for figures representing the argument of the Fourier transform. Similar images could be drawn for the modulus (or real or imaginary parts). The top-right and bottom-left figures are identical, but for the fact that the regions not transmitted by the array are excluded.

The right figure is an illustration for the densification operation described in Eq.10, in which the angular frequency transmitted by the array of telescopes are regrouped towards the lower frequencies, to simulate a monolithic aperture. The operation described in this figure corresponds to the periscopic approach. Operating a zooming of the regrouped central region would lead to the inverse Galilean approach, which is fundamentally equivalent. It is important to note that these parts of spectra are globally moved from high frequencies to low ones without alteration, as first described by Tallon & Tallon-Bosc (1992).

The operations to get the final hypertelescope images with the 25 apertures array are illustrated in **Fig.7**. In the top left figures we have represented the operation of densification of the OTF in the Fourier space, similarly to what was shown in Fig.6. Because we have now 601 regions, it is no more possible to represent the image with its full resolution as we did before, and the representations of the OTFs, before and after densification, are clipped to black and white.

The resulting filling of the Fourier plane is not as continuous as for the redundant array because the geometry of the centers of the array must remain unchanged. The gaps presents in the original OTF remains in the densified one. Note that the designation as OTF for the frequency transmission after densification is improper, because the object-image relationship no longer exists as a convolution.

In the simulation, the densification parameter γ is approximately equal to $7/3 \sim 2.34$, that is the elementary distance $d = 7$ units is reduced to $d' = 3$. The bottom left figure of Fig.7 represents the modulus of $\hat{I}'(u)$, and the bottom left figure the simulated densified image as given by Eq. 11. The resulting figure appear then as a zoom performed on the Fizeau image, as described by Aime (2008).

3.3. Photodetected focal images

In the following examples, we have $N = 1$ million, the mean number of photons per pixel is then ~ 0.95. The m_{ij} are real positive numbers that varies from 0 to a maximum of ~ 3.7, sensibly the same in the direct and densified images. There is no more photons per pixel in the densified image than in the direct image because of the zooming effect (pixels correspond to different angular units in the two images). If a de-zooming was applied, the number of photons per pixel in the densified image would increase as γ^2, i.e. a factor of about 5.4. The interest for the densification would be more obvious if γ could be larger, but this would also require an increase in the number of pixels in the images, and a correlative increase in time in the application of RLA.

With the procedure we used, the final total number of photons in the images is not exactly N, but fluctuates around N with a standard deviation of $\sqrt{N}$. The examples of photodetected images shown in **Fig.8** indeed corresponds to photon numbers of 999 960 and 999 355, an irrelevant difference with $N = 1$ million for a fair comparison between the two images.

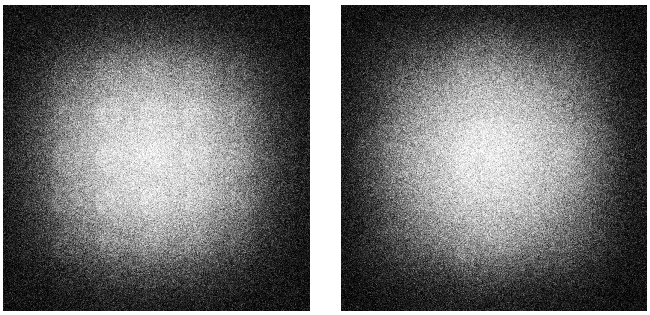


Fig. 8. Photodetected focal images corresponding to direct (left) and densified (right) images of Fig.3, top right, and Fig.4, bottom right, respectively. The number of photons in each image is approximatively 1 million.

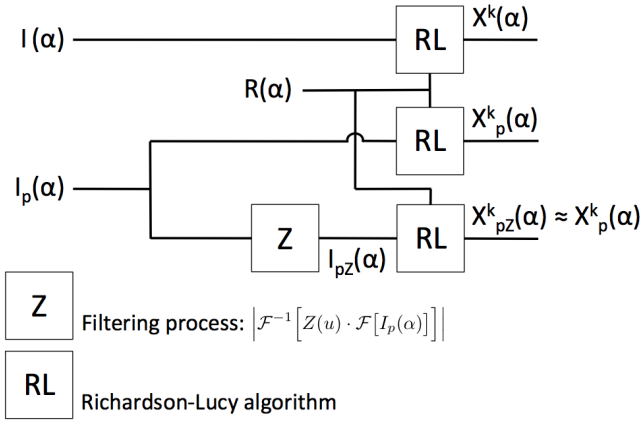


Fig. 9. Block-diagram of the application of RLA on Fizeau interferometric images. $X^k(\alpha)$ is the output at the iteration k. $R(\alpha)$ is the common PSF used to deconvolve the noiseless image $I(\alpha)$ and the photodetected image $I_p(\alpha)$ and $I_{pZ}(\alpha)$. This latter is pre-filtered by Z. The two outputs for the noisy image are similar.

4. Image enhancement using the Richardson-Lucy algorithm

4.1. Brief presentation of the Richardson-Lucy algorithm

For a Poisson noise process, the deconvolution is ideally performed by means of the Richardson-Lucy (RL) iterative algorithm (Lucy (1974), Richardson (1972)), an algorithm that follows the more general approach of the Expectation Maximization (EM) algorithm [Dempster et al.1977], Rubin (1977). It has been shown that this algorithm maximizes the likelihood of a Poisson noise process corrupting the data, subject to a non negativity constraint of the estimates. In an equivalent way it can be considered as an algorithm that minimize the negative

Log-likelihood that is the Kullback-Leibler divergence between the noisy data and the convolutive linear model (eq.2, subject to non negativity constraint.

In a relaxed form the algorithm writes

$$X^{k+1}(\alpha) = X^k(\alpha) + \beta^k X^k(\alpha) \times R(-\alpha) * \left(\frac{I_p(\alpha)}{R(\alpha) * X^k(\alpha)} - 1 \right) \quad (12)$$

where $X^k(\alpha)$ is the estimate at the iteration k for the object $O(\alpha)$ we seek to recover, and the parameter β^k is a descent step size ensuring the convergence of the algorithm (Lantéri et al. (2002)). If the step size is set to 1 for all k, we recover the classical multiplicative form proposed by Richardson [ ] and Lucy [ ]

$$X^{k+1}(\alpha) = X^k(\alpha) \times R(-\alpha) * \frac{I_p(\alpha)}{R(\alpha) * X^k(\alpha)} \quad (13)$$

The convergence of such simplified form has been demonstrated [ ]. The iterative process generally starts with an initial estimate $X^0(\alpha)$ whose value is a constant equal to the mean of $I_p(\alpha)$.

The effect of this algorithm is well known when the PSF $R(\alpha)$ corresponds to a low pass filter. Roughly speaking, during the iterative process, the low spatial frequencies are reconstructed first and the higher frequencies appear progressively when the iteration number increases. The main drawback of such iterative algorithm as well as all the others deconvolution algorithms lies in the fact that the deconvolution problem is an ill posed problem [Bertero and Boccacci, Livre], and as a consequence when the iteration number increases too much, the reconstructed image becomes very noisy. To avoid this problem, the classical ways to solve this problem are either to regularize explicitely [Lanteri et al. 2002] the problem by introducing at some level, a smoothness penalty, or to stop the iterative process before noise amplification. We will see in the simulation that the effect of RL on interferometric images is more complex.

4.2. Application of RLA to interferometric images obtained in the Fizeau mode

The block-diagram shown in Fig.9 describes the application of the RLA to the interferometric images $I(\alpha)$ and $I_p(\alpha)$, i.e. to the upper outputs of the block-diagram of Fig.1. The result of the processing of $I(\alpha)$ with RLA is denoted $X(\alpha)$ there for generality. This algorithm realizes the deconvolution of the observed image knowing the PSF $R(\alpha)$. In the present study, no explicit regularization is used, and the output $X^k(\alpha)$ is parametrized by the number of iterations k performed with the iterative algorithm, as shown in Eq.12 and Eq.13.

For $I_p(\alpha)$, the diagram has two lanes. One corresponds to the direct application of RLA to the raw photodetected image, and the other is the application of RLA after the application of a prefilter that is noted Z in the representation. This operation is a simple application of a filter in the Fourier plane whose effect is to reduce the influence of photon noise on the direct photonized image. As we will see its interest is essentially in relation with the processing of hypertelescope images. What we show here is the insensitivity of the RLA to this filter, the application of which will be mandatory in the hypertelescope case.

4.2.1. Noiseless images

As already indicated in the previous section, the RLA is an algorithm that was generated assuming Poisson noise. Here we consider its application to the noiseless image $I(\alpha)$, to check its capability to recover missing parts of the frequency spectrum. One could consider noiseless data as the limit of a Poisson process for a very large number of photons. **Otherwise, Dempster et al. consider this algorithm for missing data (reformater).**

We start with the image $I(\alpha)$ shown in Fig.5 for the data obtained with $d = 7$, the central 256×256 pixels of which is shown in **Fig.10** (top, left). However, it should be noted that the algorithm is applied to the whole 1024×1024 image, and that the central part of the image is shown here only for comparison with the results.

We have run the RLA up to $k = 30000$. After a few hundred of iterations, the replicas in the original image disappear and only a single central image of the Earth-like object remains. The recovery of small details of the astronomical object requires a larger number of iterations (a few thousands). Two steps of the images $X^k(\alpha)$ for the iterations $k = 100$ and $k = 30000$ are given in Fig.10. The original image is given in the same figure for comparison. As a result the quality of the image seems to increase monotonically with the number of iterations. After $k = 5000$ or so, the image improvement is very slow. Possible numerical instabilities, not observed up to $k = 30000$ using *Mathematica* may limit the image enhancement for the noiseless image. A limitation is the time to run the program (about one day of computation with a MacBook Pro for $k = 30000$).

The way RLA is deleting replicas is better understood in the Fourier plane, as we illustrate it in **Fig.11**. The RLA is a non-linear algorithm whose property to extend the frequency spectral range of the image is well known (**ref par exemple: Comparison between ISRA and RLA algorithms. Use of a Wiener Filter based stopping criterion Lanteri Soummer Aime 1999**). As the number of iterations increases, the RLA is spreading energy into missing zones of the spectrum, thus populating the gaps between the known frequencies regions. The angular frequencies coverage seems to grow preferentially from known spectral regions, and the description of a simple from low to high frequencies behavior of RLA is a bit simplistic.

In some sense, we can conclude that RLA is inpainting the image spectrum. This property have consequences in the choice of an array configuration, a point that is not examined in the present study and will be done in a future work. This inpainting that propagates from known regions tends to produce a continuous coverage of the Fourier space, at least in the dense part of the MTF, where the regular grid sampling is clear. The effect of RLA is to transform the regular sampling responsible for the peaks in the PSF, as shown in Fig.5 into an uniform coverage. Considering a Fourier transform of it, the equivalent PSF tends to present a single compact response. In other words, one can consider that the RLA has performed algorithmically the operation of densification sought with an hypertelescope. The effect of the algorithm goes beyond filling the inner areas known and extends into higher frequencies.

The result for the array with $d = 7$ is excellent, as proven by the comparison between the result $X^{30000}(\alpha)$ and the true image in Fig.10. This array assure a good sampling of the Fourier space, at least in the low frequency parts. Now we check the possibilities of the algorithm for the array with $d = 14$, covering twice as much of the spectrum, but with the drawback of a sampling twice as distant. The task for RLA is indeed more difficult. As already shown in Fig.5, the Earth images overlap one another. **Fig.12** show for this configuration the results that can be obtained with 1000 and 30000 iterations. The result of the RLA remains very good, because it seems able to partly extricate the superimposition of replicas. Nevertheless, the results are not as

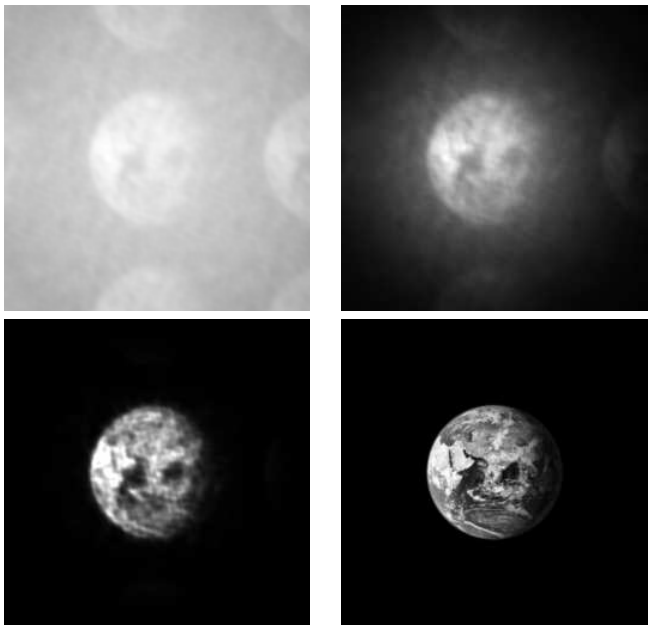


Fig. 10. Top left: central part of the direct focal plane image (noiseless). Top right: same region after 100 iterations of RLA. Bottom left: same region after 30000 iterations of RLA. Bottom right: original object.

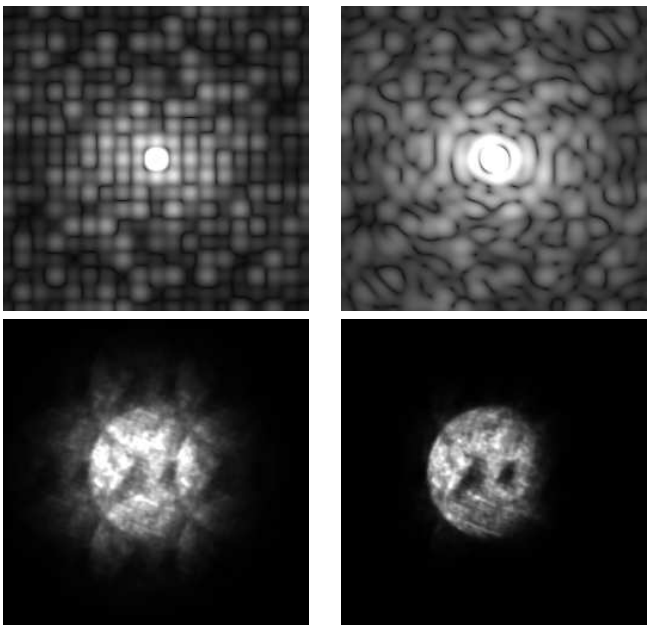


Fig. 12. Top: modulus of the spectrum. Bottom: reconstructed image. Number of iterations: 1000 (left) and 30000 (rigt). Results for a distance $d = 14$ pixels.

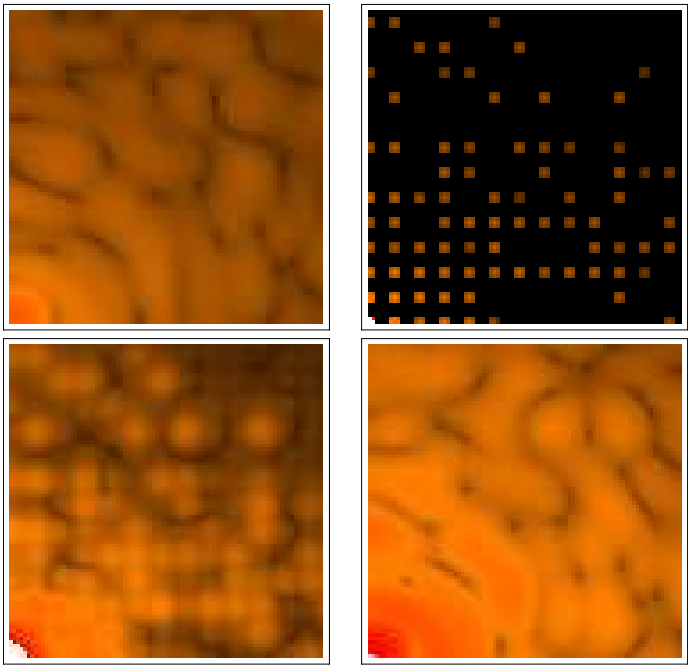


Fig. 11. Modulus in the Fourier space of a small central region (u_x and $u_y \geqslant 0$). Top left: $|\hat{O}(u)|$, Top right $|\hat{I}(u)|$, Botom: left result for $k = 100$, right for $k = 3000$. Results are for the 25 non-redundant array with $d = 7$.

good as for $d = 7$. Although the $d = 14$ array has a resolving power twice as large as the $d = 7$ one in the sense usually utilized for interferometry, the winner of the comparison is the smaller array. Of course this is fully object dependent, and an adequacy between the array and the object must be ensured.

Introduire distance si possible.

4.2.2. Photodetected image

For the photodetected image, the fluctuations present in the image due to the Poisson process are amplified during the iterations. A good but delicate technique is to apply a regularization term to the algorithm (REFERENCES). Alternatively a simple way is to stop the iterations. Because we are dealing with a full simulation (we know the object $O(\alpha)$), we can measure the goodness of the image $X^k(\alpha)$ by computing a distance between ideal and reconstructed images. In **Fig.13** we have drawn the Euclidean distance

$$E(k) = \int |X^k(\alpha) - O(\alpha)|^2 d\alpha, \tag{14}$$

as a function of the iteration number k. For the chosen example, there is a flat minimum around the iterations 500 to 700. An example of the reconstructed images for several k values is shown in **Fig.14** .

Commenter un peu ces figures.

Now we consider the application of RLA to a pre-filtered image, as indicated in the block-diagram of Fig.9. As already indicated in the introduction of this section, the pre-filter we use here is for further application in the hypertelescope case. Let us first describe it. We know that because the photodetection is a Poisson process, a white noise will be superimposed to the image spectrum. Since we know the domain of frequencies transmitted by the array of telescopes, it is conceivable to filter this noise in the region of the spectrum where no signal is expected. For that, we can multiply the spectrum by the indicator function of the MTF $T(u)$, a function equal to 1 for $T(u) \neq 0$, and 0 elsewhere.

In practice this indicator function is obtained applying a signum function to the absolute value of $T(u)$. We denote as $Z(u) = \text{sign}(|T(u)|)$ this function. An illustration of the application of the indicator function to the image spectrum is shown in **Fig.15**. The filtered direct image is $I_{pZ}(\alpha) = |\mathcal{F}^{-1}[Z(u)\hat{I}_p(u)]|$, taking the absolute value of the final image to get rid of any very small non real-positive values. The filtered image result is shown

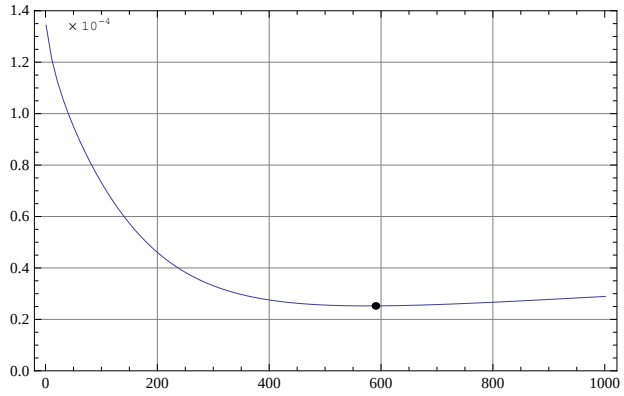


Fig. 13. Error term representing the Euclidean distance written in Eq.14 for the interferometric image shown in Fig.8. The minimum is around $k = 590$.

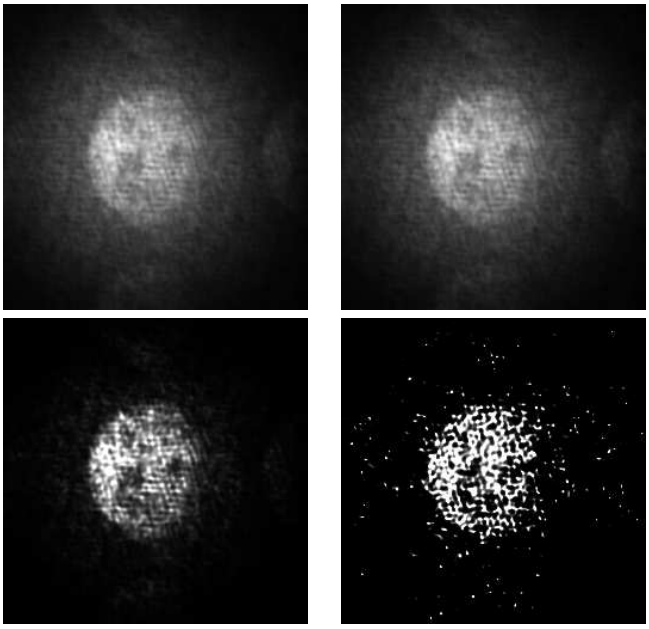


Fig. 14. Result of the application of RLA to the interferometric image shown in Fig.8. Top: for direct $X_p^{100}(\alpha)$ image (left) and pre-filtered $X_{pZ}^{100}(\alpha)$ image (right). Bottom: result for $X_p^{590}(\alpha)$ (left) and $X_p^{20000}(\alpha)$ (right).

in the figure. It seems to produce a great improvement of the direct image shown in Fig.8. In fact, after application of the RLA, the results are quite similar, both for the error curve than for the reconstructed images. The results are similar enough not to be reproduced here because they will appear as duplicated figures. This result is not surprising because RLA is the reconstruction algorithm optimized for Poisson noise, and there is no improvement to be expected from a pre filter. From this experiment, however, we deduce that the pre-filter does not degrade the images when applying RLA. As already indicated, this result will be interesting for the treatment of hypertelescope images.

In Fig.15 we have anticipated the application of the same kind of filter to the photodetected image. For the densified image, we denote as $Z'(u)$ the indicator function of $Z(u)$ after densification, i.e. a low pass version of it. The filtered densified image is $I'_{pZ}(\alpha) = |\mathcal{F}^{-1}[Z'(u)\hat{I}'_p(u)]|$. The result of this operation on the densified images is also given in Fig.15.

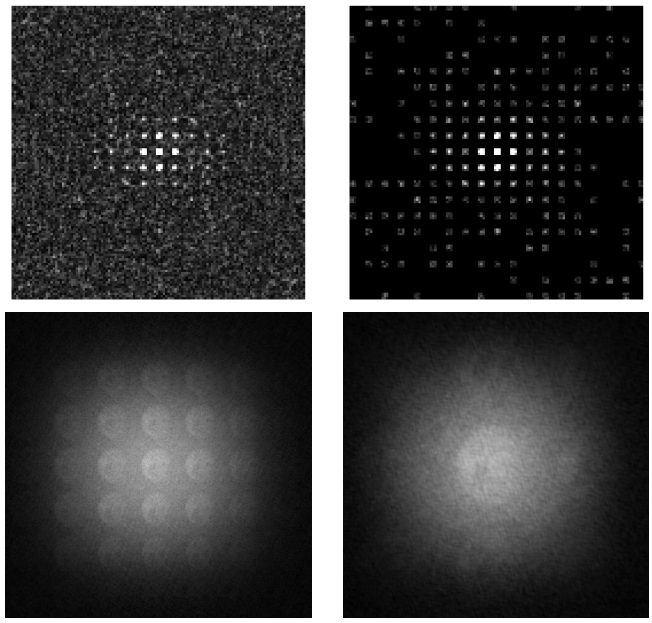


Fig. 15. Top: modulus of a central 128×128 region of the spectrum of the direct image of Fig.8 before (left) and after (right) application of $Z(u)$. Bottom left: result on the image. Bottom right: result for the densified image after the application of the same procedure.

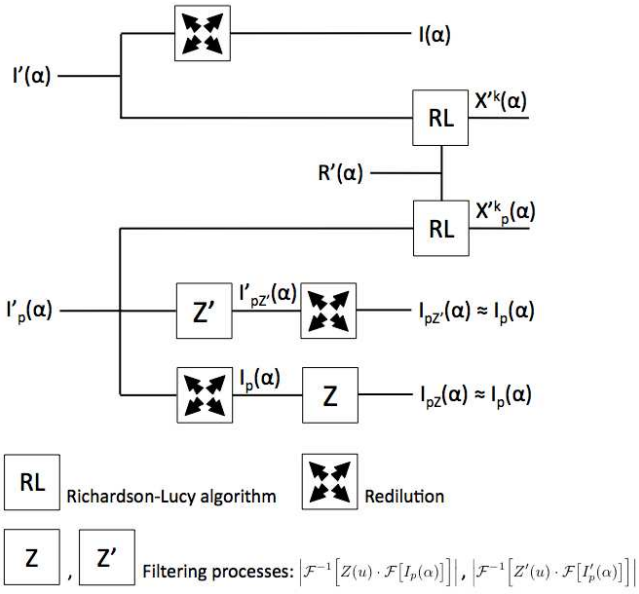


Fig. 16. Block-diagram of the application of RLA on hypertelescope images. After MTF redilution, $I'(\alpha)$ becomes equal to $I(\alpha)$ of the block-diagram of Fig.9. $R'(\alpha)$ is the pseudo PSF used to deconvolve the densified images and that is applied both to $I'(\alpha)$ and to $I'_p(\alpha)$. The two bottom lanes of the diagram represent equivalent operation involving the application of the MTF redilution and filter Z. The filter Z' is the densified version of Z. The two outputs for these processed densified images are similar to $I_p(\alpha)$.

4.3. Application of RLA to hypertelescope images

The block-diagram of Fig.16 describes the operations that can be applied to the densified images $I'(\alpha)$ and $I'_p(\alpha)$. It shares with the block-diagram of Fig.9 the decomposition of the two lanes, one for the noiseless image and one for the photodetected images. It differs from it on several points, $R'(\alpha)$ is substituted to $R(\alpha)$ for

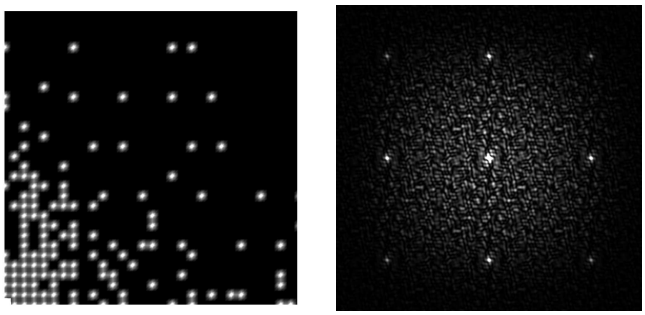


Fig. 17. Hypertelescope Left: pseudo MTF, the zone shown here is the same as in Fig.11. Right: pseudo PSF.

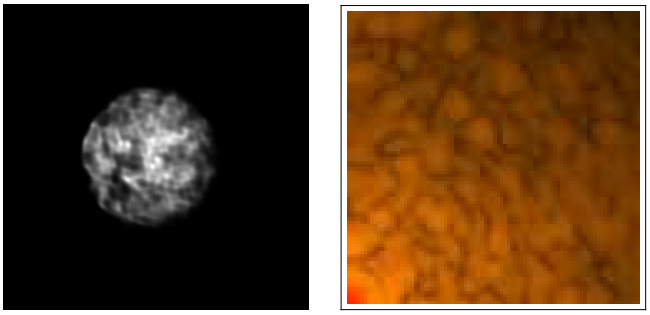


Fig. 18. Left: changer image. Right: result of the application of the RLA (monter comme dans figure 11).

the application of RLA, there is a pre-filter Z', and mainly because there is a new operation called *redilution*. The alert reader will have already noted that some operations indicated in this block-diagram are somewhat problematic.

The major problem concern the possibility of implementing a deconvolution of the hypertelescope images. Indeed the hypertelescope produces an image that is not the result of a convolution, but that of a more complex process, as described before. What sense can we give to the deconvolution of a relation that is not a convolution? At that level, one could conclude that RLA, as a deconvolution algorithm, cannot be applied to a densified image and that some other approach, still to be find, should be used to improve these images.

We tried to overcome this difficulty as follows. We assume with Labeyrie (2007) that the densification performs a pseudo-convolution. To apply RLA we need to have a PSF. For that, we take as the pseudo transfer function the densified form of the MTF, and deduce from it a pseudo PSF, using a Fourier transform. The densified MTF $T'(u)$ and PSF $R'(\alpha)$ are given in Fig.17. This operation is what it is worth, but what else to do?

Fig.18 shows the output of RLA $X'^k(\alpha)$ for $k = 5000$. The result is very disappointing, but not unexpected. The modulus of the spectrum is also given in the figure. The fact that we have densified the aperture, and therefore the MTF, leaves no room for RLA to reconstruct missing frequencies.

An alternative is to invert the densification process to recover the relation of convolution that a deconvolution program such as RLA can handle. The technique of redilution was already described in Tallon & Tallon-Bosc (1992) and in Guyon & Roddier (2002) for coronagraphic applications, for example. Because here we have made a densification of the MTF, and not of the apertures, the redilution can be performed without any loss of signal.

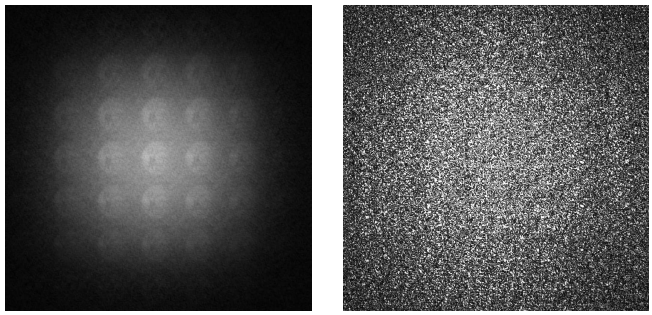


Fig. 19. Left: hypertelescope image after MTF redilution. Right: absolute difference between this image and the interferometric image shown in Fig.**??**. Differences are due to statistical origin of the photodetection process.

The procedure for image redilution is just the inverse of what was illustrated in Fig.6 and Fig.7. For the noiseless image, we start with the image $I'(\alpha)$, compute its Fourier transform and perform the reverse operation of the densification, i.e. blocks of frequencies moved from the central position u_{kl} to the lower frequency u'_{kl} in the densification procedure are now shifted back to their original position u_{kl}. In these conditions, an image obtained at the focus of the hypertelescope can be readily transformed in an image strictly equal to the Fizeau interferometric image. This is why in the block-diagram of Fig.16 we recover $I(\alpha)$ from $I'(\alpha)$, and the data processing of this image call back to Fig.9.

The application of RLA to the photodetected image $I'_p(\alpha)$ gives poor results as previously for the noiseless image (reverifier une derniere fois) and is not shown here (ou montrer). The alternative is here also to apply the image redilution. In this case it seems mandatory to utilize a filter such as $Z(u)$. Indeed, the image spectrum $\hat{I}'(u)$ is contaminated by photon noise, and the operation of redilution in witch frequency regions will be translated from low to higher frequencies can only concern the regions transmitted by the telescope array. We cannot handle the redilution of the photon noise spectrum, and the best we can do seems to replace it by zero in the region of no signal. In the block-diagram of Fig.16 there are two lanes for this operation, both leading to an identical result. The reason of that is that the application of an indicator function such as $Z(u)$ can be equivalently made before of after redilution (we have denoted as $Z'(u)$ the low frequency version of the pre-filter $Z(u)$).

The rediluted and pre-filtered images, shown in **Fig.19** (left image), appears very similar to the pre-filtered Fizeau image $I_{pZ}(\alpha)$ of Fig.15. The difference between them, shown in absolute value in the right image of Fig.19 corresponds to fluctuations due to the Poisson statistics. SInce we have proven above that RLA gives equivalent results for $I_{pZ}(\alpha)$ or $I_p(\alpha)$, we have then obtained a modus to process hypertelescope images.

5. conclusion

cette approche peut etre utilisee pour tester les configurations de telescopes sur un critere objectif, apres dcv

References

Aime, C. 2008, A&A, 483, 361
Guyon, O. & Roddier, F. 2002, A&A, 391, 379
Labeyrie, A. 1975, ApJ, 196, L71
Labeyrie, A. 1996, A&AS, 118, 517
Labeyrie, A. 2007, Comptes Rendus Physique, 8, 426

Lantéri, H., Roche, M., & Aime, C. 2002, Inverse Problems, 18, 1397
Lardière, O., Martinache, F., & Patru, F. 2007, MNRAS, 375, 977
Lucy, L. B. 1974, AJ, 79, 745
Michelson, A. A. 1920, ApJ, 51, 257
Michelson, A. A. & Pease, F. G. 1921, ApJ, 53, 249
Mourard, D., Clausse, J. M., Marcotto, A., et al. 2009, A&A, 508, 1073
Mourard, D., Tallon-Bosc, I., Blazit, A., et al. 1994, A&A, 283, 705
Ohnaka, K., Weigelt, G., Millour, F., et al. 2011, A&A, 529, A163+
Patru, F., Mourard, D., Clausse, J.-M., et al. 2008, A&A, 477, 345
Patru, F., Tarmoul, N., Mourard, D., & Lardière, O. 2009, MNRAS, 395, 2363
Richardson, W. H. 1972, Journal of the Optical Society of America (1917-1983), 62, 55
Rubin, A. P. D. N. M. L. D. B. 1977, Journal of the Royal Statistical Society. Series B (Methodological), 39, 1
Tallon, M. & Tallon-Bosc, I. 1992, A&A, 253, 641
ten Brummelaar, T. A., McAlister, H. A., Ridgway, S. T., et al. 2005, ApJ, 628, 453